



# Poly(maleic acid-co-acrylic acid) ionomer as nucleating agent on the crystallization behavior and properties of poly(ethylene terephthalate)

Wei Zhang<sup>1</sup> · Hongdong Zhang<sup>1</sup> · Yuliang Yang<sup>1</sup> · Ping Tang<sup>1</sup>

Received: 2 November 2020 / Revised: 9 March 2021 / Accepted: 16 March 2021

© The Author(s), under exclusive licence to Springer-Verlag GmbH Germany, part of Springer Nature 2021

## Abstract

Polyethylene terephthalate (PET) generally suffers from low crystallization rate and long molding cycle, which limits its application in injection molding of engineering plastics. To overcome the specific shortcoming, polymaleic acid-co-acrylic acid (PMA-AA) ionomer used as a nucleating agent was added to PET by melt blending, and its effect on the crystallization behavior of PET was investigated in this paper. It is indicated that the modified PET samples (MPET) with the addition of nucleating agents exhibit much higher molecular order and faster crystallization rate. The nucleation mechanism of MPET induced by PMA-AA ionomer was analyzed by means of Avrami equation and Hoffman–Lauritzen theory, revealing that the addition of PMA-AA ionomer provides more nucleation sites and reduces the fold surface free energy of PET. The nucleation and dispersion behavior of PMA-AA ionomer were further observed by SEM and POM morphologies. The results demonstrated that ionomer was dispersed homogeneously in the PET matrix, thus leading to faster crystallization rate of MPET than neat PET. In addition, the thermal stability, mechanical properties, and gas barrier of PET and MPET were characterized.

## Introduction

PET is a semicrystalline thermoplastic material with a variety of outstanding physical properties such as high tensile strength, excellent thermal stability, attractive electrical insulation, and extremely low gas permeability [1–6]. As a result, it is widely applied in fibers, bottles, industrial films, and engineering plastics [7–10]. However, the rigid conjugated structure impedes the movement of its molecular chains in the crystallization transition of PET and results in a decline in its crystallization performance. This issue greatly extends its molding cycle

✉ Ping Tang  
pingtang@fudan.edu.cn

<sup>1</sup> State Key Laboratory of Molecular Engineering of Polymers, Department of Macromolecular Science, Fudan University, Shanghai 200433, China

due to the requirement of high temperature of mold and influences its physical properties, thus limiting its application as engineering plastics [11]. Therefore, inorganic substances like  $\text{SiO}_2$ , montmorillonite and organic salts [12, 13] such as aromatic alkali metal salt [6, 14, 15] have been used as nucleating agents to improve the crystallization of PET [16, 17]. However, most nucleating agents behave poor dispersion in the PET matrix due to the inferior compatibility with PET, which ultimately weakens the physical and chemical properties of the blends.

Ionomer is a polymer material with a small quantity of ionic groups either along the polymer backbone chains or as pendant groups. The added ionomers which have superior compatibility with PET such as containing reaction group with PET normally cause a slight decrease in the molecular weight of PET [18–21]. Since ionomer not only can provide PET with nucleus, but also the quite flexible chain can speed up the movement of PET chain to accelerate the crystallization rate [22, 23]. Consequently, the suitable ionomer has been recognized as the most effective PET nucleating agent in the industry. For example, it has been reported that ethylene-sodium methacrylate copolymers (Surlyn) [24], ethylene-sodium acrylate copolymers (AClyn) [22] and other ionomers [25–27] have been used as nucleating agents to enhance the crystallization rate of PET. Polymaleic acid-co-acrylic acid (PMA-AA) is a linear polymer containing carboxyl groups with simple synthesis method and high yield. Recently, it has been widely applied as washing aid, scale inhibitor and water-resistant membrane [28–30]. The polymer chain of PMA-AA ionomer is stretched due to the electrostatic repulsion between the molecular chains and the side groups in the molecular chain; hence, the ionomer can be evenly dispersed in the PET matrix and react as an effective nucleating agent.

PET/ionomer blends were obtained by melt blending method, in which PMA-AA ionomer was dispersed in PET matrix as an organic nucleating agent with a certain weight ratio, such as 0.5 wt%, 1.0 wt%, 2.0 wt%, and 5.0 wt%. The structure of PMA-AA ionomer was characterized by Fourier transform infrared spectrometer (FTIR) and carbon nuclear magnetic resonance ( $^{13}\text{C-NMR}$ ). The effect of different compositions of PMA-AA ionomer on the disperse in the PET matrix and the crystallization behavior of PET was investigated by differential scanning calorimetry (DSC), scanning electron microscope (SEM), and polarized optical microscopy (POM). In our previous work [25, 26], polystyrene-co-maleic anhydride (SMA) ionomers were designed as nucleation agents to improve the crystallization behavior of PET, but the study of non-isothermal crystallization and physical properties was not explored further. In this work, PMA-AA ionomer was used as a new type of nucleation agent, and the crystallization of PET/PMA-AA ionomer blends was comprehensively analyzed both by non-isothermal crystallization and isothermal crystallization. The nucleation mechanism of PET with the addition of the ionomer was further analyzed by means of Avrami equation and Hoffman–Lauritzen theory. Furthermore, the physical and chemical properties including thermal stability, mechanical properties, and gas barrier behavior of PET/ionomer blends were investigated in detail for potential applications in engineering plastics.

## Materials and experiments

### Materials

Polyethylene terephthalate (PET) with intrinsic viscosity of 0.79 dL/g was acquired by Zhejiang Wankai New Material Company limited, China. Commercialized PMA-AA copolymer (trade name 416,053) was purchased from Sigma-Aldrich. Commercialized PMA-AA ionomer (trade name PMAS-90) was produced by BASF. Other chemicals were purchased from the Sinopharm Chemical Reagent, and all of them were analytical grade and used without further purification.

### Preparation of PET/ionomer blends

Firstly, the purchased ionomer was dissolved in deionized water and then precipitated in a mixed solution of acetone and ethyl acetate, repeating this approach at least three times to ensure the purification. The final products were dried at 50 °C in the vacuum oven for 24 h and ground into powder for further use. PET was dried at 110 °C for at least 24 h in the vacuum oven before use to prevent hydrolysis during the melt processing. Then, PET was mixed with PMA-AA ionomer in the Changkai CTR-300 torque rheometer made in China at 280 °C at the speed of 60 rpm for 5 min and then crushed into small particles in a universal crusher for further study. Corresponding to the type and ionomer content, samples were named as neat PET and MPET series, as shown in Table 1.

### Characterization techniques

The FTIR spectra were recorded on Nicolet 6700 (ThermoFisher, the USA) with DTGS detector at wavenumber between 400 and 4000 cm<sup>-1</sup> and with 64 scans being taken at 4 cm<sup>-1</sup> spectral resolution. The <sup>13</sup>C-NMR spectra were recorded on Avance III HD (Bruker, Switzerland) at 25 °C with D<sub>2</sub>O as solvent at a resonance frequency of 500 MHz.

The non-isothermal and isothermal crystallization behaviors were investigated by DSC Q2000, TA instruments in the nitrogen atmosphere. The calibration was conducted with standard indium. The SEM images were investigated by a Zeiss Ultra 55 at 20 kV with a working distance of 7 mm. The sample was free-fractured and

**Table 1** Sample code, ionomer, and its content in PET

	Sample	Ionomer	Ionomer content (wt%)
1	PET	None	0.0
2	MPET-0.5	PMA-AA-Na	0.5
3	MPET-1.0	PMA-AA-Na	1.0
4	MPET-2.0	PMA-AA-Na	2.0
5	MPET-5.0	PMA-AA-Na	5.0

coated with gold to enhance conductivity. In situ optical micrographs were obtained with the POM (Olympus BX51, Olympus Optical Co., Ltd., Japan) with a hot-stage THMS-600 (Linkam, the UK), and video camera was used to record the crystal formation.

The thermal stability behavior of PMA-AA ionomer was measured by using thermogravimetric analyzer (TGA) Pyris1 (PE instrument, the USA). The mechanical properties were measured by electronic universal testing machine Instron 5966, and the results are the average of five measurements per sample. The oxygen permeation measurements were taken using a Basic 202 (Labthink, China) equipped with an oxygen sensor at 23 °C, which can directly measure the oxygen transmission rate.

## Results and discussion

### Characterization of PMA-AA and its ionomer

Figure 1 shows FTIR spectra of PMA-AA with assigned structural features, referring to the literature [28]. The strong absorption peaks at 1582–1401 cm<sup>-1</sup> indicate the carbonyl group. The peaks at 3417 cm<sup>-1</sup> represent the absorption of hydroxyl group on carboxyl group. The peaks at 2950 cm<sup>-1</sup> correspond to methine in the polymer chain. Therefore, it can be confirmed that the polymaleic acid-co-acrylic acid (PMA-AA) copolymer has been synthesized successfully. The shape of the peak at 1125 cm<sup>-1</sup> in PMA-AA-Na becomes wider and higher compared to PMA-AA copolymer, indicating that polymaleic acid-acrylic acid was partially hydrolyzed to the ionomer.

From <sup>13</sup>C-NMR spectra of PMA-AA copolymer shown in Fig. 2, the chemical shift of characteristic carbons in maleic acid and acrylic acid was marked in the spectrum. There are four kinds of carbon atoms in the main carbon chain structure. The chemical shift of carbon in the acrylic acid without connecting the carboxyl group appears at about 36 ppm. The two kinds of carbon in the middle of the main chain are concentrated and appear at about 46 ppm due to the symmetrical chain

**Fig. 1** FTIR spectra of PMA-AA and its ionomer

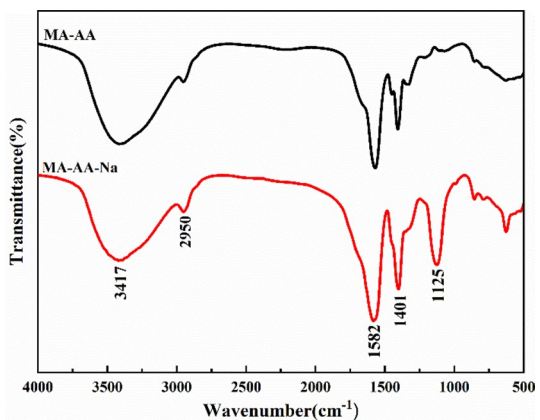
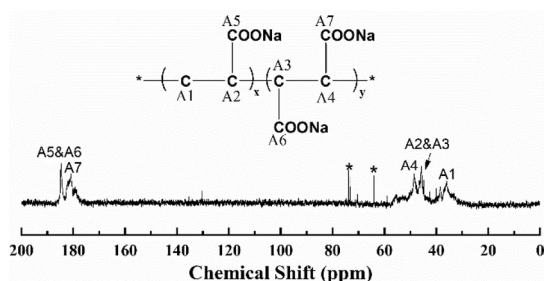


**Fig. 2**  $^{13}\text{C}$ -NMR spectra of PMA-AA ionomer with peak assignments



structure. The peak at 48 ppm corresponds to the other carbon in the maleic acid. Therefore, it can be confirmed that PMA-AA ionomer was successfully synthesized.

### Non-isothermal crystallization behavior of PET and MPET blends

In the actual production process, the crystallization behavior of polymers is mostly non-isothermal case; thus, the investigation of non-isothermal crystallization of polymers has great practical significance. To explore the non-isothermal crystallization and melting behavior, the samples with 8–10 mg were heated to 285 °C at a rate of 10 °C/min and maintained for 5 min to erase the previous thermal history on the hot stage and then quenched in liquid nitrogen to guarantee the amorphous state of PET and MPET samples. Non-isothermal crystallization includes: firstly, the amorphous samples are heated from the glass state at the room temperature, and the crystallization process occurs during the heating process, which is so-called cold crystallization. During the heating process, the glass transition temperature  $T_g$ , cold-crystallization temperature  $T_{cc}$ , and melting temperature  $T_m$  of the sample can be measured. Secondly, the sample is cooled from the molten state to the room temperature at a fixed cooling rate, where the melt crystallization occurs. During the melt crystallization process, the onset crystallization temperature  $T_{onset}$ , melt-crystallization temperature  $T_{mc}$  and the enthalpy of melt-crystallization  $\Delta H_{mc}$  can be measured. The most intuitive parameters for judging the crystallization ability of a sample are the cold-crystallization temperature  $T_{cc}$  and the melt-crystallization temperature  $T_{mc}$ . Lower  $T_{cc}$  and higher  $T_{mc}$  values indicate that cold crystallization and melt crystallization are more prone to occur. In addition, we can compare the crystallization rate of the sample by the half width  $W_{1/2mc}$  of the melt-crystallization peak. It is noted that the temperature and peak shape of phase transitions such as glass transition, cold crystallization, melting process, and melting crystallization are related to the heating/cooling rate and the addition of nucleating agent.

Figure 3 shows non-isothermal crystallization curves on PET and MPET samples at the heating/cooling rate of 10 °C/min, and the significant parameters extracted from the figures are listed in Table 2. As clearly shown in Fig. 3a, the value of  $T_{cc}$  tends to lower temperature with the addition of PMA-AA-Na compared with PET at the same cooling rate. At the same time, Fig. 3b shows that the values of  $T_{onset}$  and  $T_{mc}$  shift to higher temperature compared with PET at the same cooling rate, and the half width of exothermal peak of samples also becomes narrower with the addition

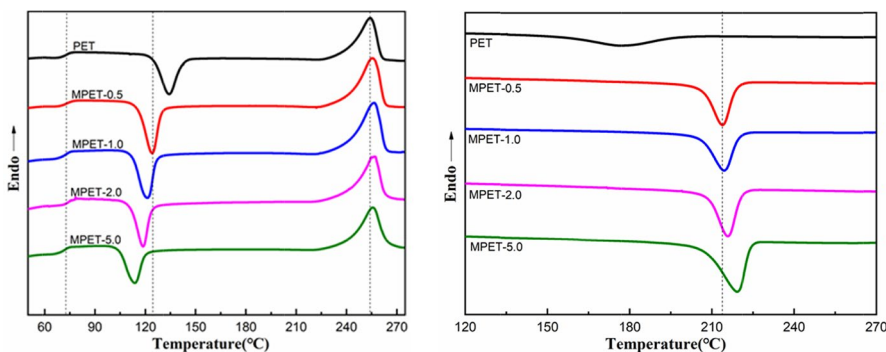


**Fig. 3** Non-isothermal melting behaviors (a), crystallization behaviors (b) of PET and MPET with heating and cooling rate of 10 °C/min

**Table 2** Non-isothermal melting and crystallization parameters for PET and MPET blends

Samples	$T_g$ °C	$T_{cc}$ °C	$T_m$ °C	$\Delta H_m$ J/g	$T_{onset}$ °C	$T_{mc}$ °C	$W_{1/2mc}$ °C	$\Delta H_{mc}$ J/g	$\Delta T_{mc}$ °C	$X_C\%$
PET	72.8	134.1	254.3	39.6	205.8	176.8	31.8	34.7	77.5	29.5
MPET-0.5	73.4	123.9	255.4	45.7	223.6	213.8	11.6	42.3	41.6	36.0
MPET-1.0	73.1	121.3	256.0	45.9	224.9	214.6	11.2	43.7	41.4	37.2
MPET-2.0	73.8	118.4	256.3	45.7	226.1	215.8	10.6	44.2	40.5	37.6
MPET-5.0	72.4	113.6	255.5	45.4	226.7	218.9	10.1	44.6	36.6	37.9

of PMA-AA-Na. The addition of PMA-AA-Na decreased the cold-crystallization of PET by about 10–25 °C and increased the melt-crystallization temperature by about 30–40 °C. With the increase in the amount of PMA-AA ionomer,  $T_{cc}$  becomes lower and  $T_{mc}$  becomes higher at the same time. Furthermore, the  $T_{cc}$  of PET has already decreased by about 13 °C and the  $T_{mc}$  has already increased by about 38 °C with the addition of only 1.0 wt% PMA-AA-Na.

These results clearly acknowledge that the addition of only a small amount of PMA-AA ionomer can accelerate the crystallization rate of PET and PMA-AA ionomer can act as an effective nucleating agent for PET. In general, the supercool temperature  $\Delta T_{mc}$  defined as  $\Delta T_{mc} = T_m - T_{mc}$  can be used to characterize the crystallization and nucleation effect of a sample. It is shown that  $\Delta T_{mc}$  decreases after the addition of PMA-AA-Na, indicating higher crystallization and nucleation rates for MPET. The constant relative crystallinity  $X_C$  was defined as the percentage ratio of  $\Delta H_{mc}$  to  $\Delta H_f$ , where  $\Delta H_{mc}$  is the heat of fusion and  $\Delta H_f$  is the heat of fusion reaching the equilibrium melting, and  $\Delta H_f$  for PET being 117.6 J/g [31]. At the cooling rate of 10 °C/min,  $X_C$  for PET increased from 29.5 to 36.0% for MPET-0.5 and to 37.9% for MPET-5.0. It is demonstrated that MPET has higher molecular order and crystallization rate compared to PET, which reveals that PMA-AA ionomers improve the crystallinity of neat PET at the same cooling rate. It was reported that sodium carboxylate can directly react with PET [32, 33], leading to the formation of the ionic clusters between ionomers and functional groups of PET chain [22].

Therefore, the interactions of PMA-AA ionomer with PET molecular chain might provide large amounts of nucleus sites as discussed in the DSC measurements for crystallization behavior.

According to the DSC melt crystallization curve, the heat flow is integrated with the temperature to obtain the relationship between the relativity crystallinity  $X(t)$  and the crystallization temperature. For the constant cooling process of PET with a certain rate of 10 °C/min, we can convert it into a curve of relativity crystallinity versus time according to the formula. Figure 4 shows the relationship between the relativity crystallinity of different contents of PMA-AA ionomer and temperature/time. It is seen that after adding PMA-AA ionomer to PET, the crystallization onset temperature is significantly advanced from 140 to 180 °C, and the crystallization termination temperature is also significantly advanced from 205 to 225 °C. MPET-1.0 only needs almost half of the time that PET needs to reach the maximum crystallization degree, which is 325 s for PET and 175 s for MPET-1.0, respectively. Furthermore, the semi-crystallization time  $t_{1/2}$  is obviously shortened, indicating that the addition of PMA-AA ionomer has a quite effective effect on the heterogeneous nucleation of PET.

In order to further investigate the non-isothermal melt crystallization behavior, the samples were cooled at various rates from 280 °C to room temperature and MPET-1.0 was chosen as the typical sample for comparison with PET. Figure 5 shows non-isothermal melt crystallization curves at different cooling rates for PET and MPET-1.0, and the parameters extracted from Fig. 5 are listed in Table 3. As cooling rate increased from 5 to 30.0 °C/min, the obtained  $T_{mc}$  for PET decreased from 184.4 to 172.2 °C, and  $T_{mc}$  for MPET-1.0 decreased from 219.5 to 204.0 °C. Under such cooling rates,  $X_C$  for PET reduced from 31.1 to 14.6%, while  $X_C$  for MPET-1.0 decreased from 38.9 to 32.1%. The movement of the polymer chain cannot keep up with the crystallization rate with the increase of the cooling rate; thus, a greater degree of supercooling is required to complete crystallization. As a result, the peak of crystallization temperature becomes relatively wider and shifts to the lower temperature. Such comparison demonstrates that MPET-1.0 has higher molecular order and crystallization rate compared to PET as well. At the same time, when

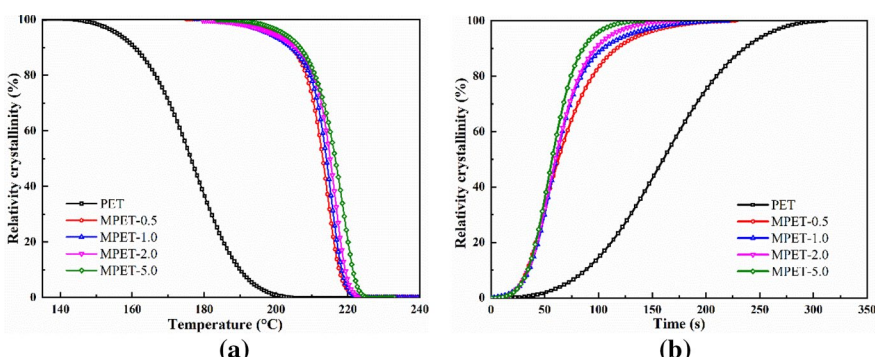


**Fig. 4** The relationship between relativity crystallinity and temperature (a), relationship between relativity crystallinity and time (b) of PET and MPET

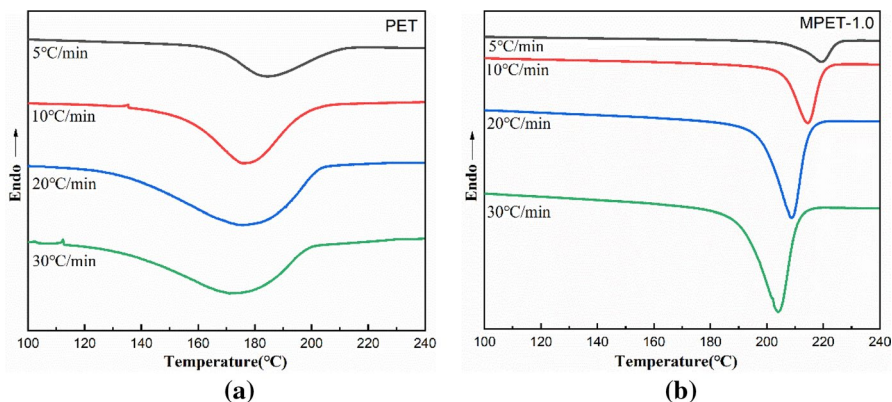


**Fig. 5** Non-isothermal melt-crystallization curves of PET (a) and MPET-1.0 (b) at different cooling rates

**Table 3** Non-isothermal crystallization parameters at different cooling rates for PET and MPET-1.0

Samples	$\Phi^a$ °C/min	$T_{\text{onset}}$ °C	$T_{\text{mc}}$ °C	$W_{1/2\text{mc}}$ °C	$\Delta H_{\text{mc}}$ J/g	$X_C$ %
PET	5	212.6	184.4	27.0	38.6	31.1
	10	205.8	176.8	31.8	34.7	29.5
	20	204.0	175.5	40.3	20.4	17.3
	30	200.6	172.2	43.0	17.2	14.6
MPET-1.0	5	227.7	219.5	10.9	45.8	38.9
	10	224.9	214.6	11.3	43.7	37.2
	20	221.2	208.9	16.5	40.3	34.3
	30	217.9	204.0	19.0	37.8	32.1

<sup>a</sup>Cooling rate

the nucleating agent is added, the nucleation sites are greatly increased and the size of the crystal particles is refined (also confirmed by the following images of crystal growth); thus, the growth of crystallization process is accelerated and the crystallization rate of PET is greatly improved.

Furthermore, the Friedman method [34] was used to calculate the activation energy, which is a function of the relative crystallinity degree  $X$  in non-isothermal crystallization, and the Friedman equation is expressed as Eq. (1).

$$\ln(dX/dt)_X = \text{const} - \Delta E_a / RT_X \quad (1)$$

The  $\ln(dX/dt)_X$  versus  $1/T_X$  plots for the neat PET and MPET-1.0 at different relative crystallinities are shown in Fig. 6. According to the Friedman equation, the activation energy at a given relative crystallinity can be obtained from the slope of the straight line of the Friedman plots and  $\Delta E_a$  of PET and MPET samples are illustrated in Fig. 7. It is obvious that the activation energy values of all PET and MPET samples increased with increasing  $X$  from 10 to 90%. The activation energy value of the neat PET varied in the finite range from  $-15.8$  to  $-5.2$  kJ/mol. In contrast,

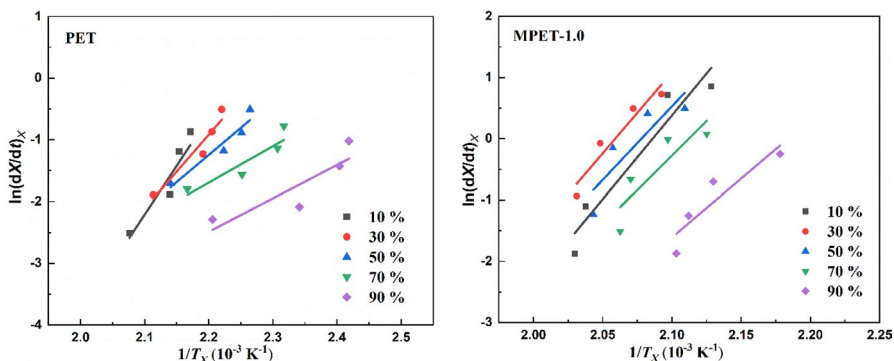
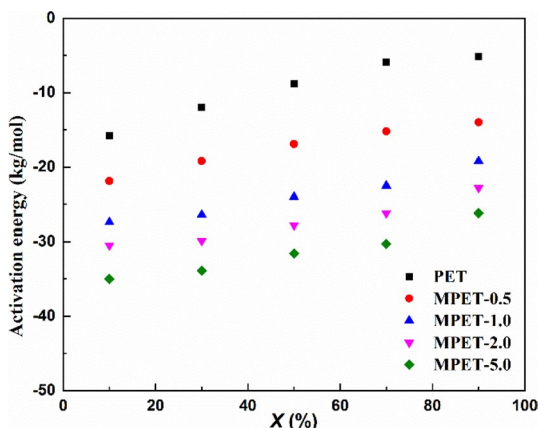


**Fig. 6** Friedman plots of  $\ln(dX/dt)_X$  versus  $1/T_X$  for PET and MPET-1.0

**Fig. 7** Dependence of the activation energy on the relative crystallinities for PET and MPET



the calculated activation energies are from  $-21.9$  to  $-14.0$  kJ/mol, from  $-27.4$  to  $-19.2$  kJ/mol, from  $-30.8$  to  $-22.8$  kJ/mol, from  $-35.0$  to  $-26.2$  kJ/mol for MPET-0.5, MPET-1.0, MPET-2.0, and MPET-5.0, respectively. These results suggest that the crystallization process easily proceeded at the initial stage of crystallization, while it becomes more difficult when reaching a higher crystallinity. In addition, an obvious decrease in the activation energy values for all MPET samples compared with neat PET and the addition of MA-AA-Na resulted in a decrease of activation energy in a dose-dependent manner. It is confirmed that MA-AA-Na can act as a heterogeneous nucleation agent to accelerate the crystallization process of the PET and promote the formation of crystals.

### Isothermal crystallization behavior of PET and MPET blends

To observe the isothermal crystallization, the samples were heated to  $285$  °C for  $5$  min to erase the previous thermal history as well, and then, samples were rapidly cooled to a fixed crystallization temperature  $T_c$  at a rate of  $100$  °C/min and

isothermal at that temperature for at least 60 min to ensure the complete crystallization of samples. The change in enthalpy with time during the isothermal crystallization was recorded at different target crystallization temperatures  $T_c$ . Then, the samples were subsequently heated to 285 °C at a heating rate of 10 °C/min to investigate the corresponding melting behavior. The melting temperature  $T_m$  and the enthalpy of fusion  $\Delta H_m$  of the samples were calculated according to the peak temperature and the area under the endothermic peak, respectively. The Avrami analysis is the most widely applied theoretical method, which can analyze the nucleation mechanism and compare the crystallization rate of polymers. Equation (2) is commonly termed as the Avrami [35, 36] equation:

$$\ln\{-\ln[1 - X(t)]\} = n \ln t + \ln K_t \quad (2)$$

where  $X(t)$  is the constant relative crystallinity at different fixed crystallization times, the  $n$  is usually termed as Avrami exponent depending on the type of nucleation and the dimension of growth, and the parameter  $K_t$  is a crystallization kinetic constant concerning both nucleation and the growth rates. From a graph  $\ln\{-\ln[1 - X(t)]\}$  versus  $\ln t$  according to Eq. (2),  $n$  is the slope of the straight line and the natural logarithm of crystallization kinetic constant  $\ln K_t$  is the intercept of the line. The area of  $X(t)$  from 0.02 to 0.3, namely the middle period of crystallization, was selected in this article for the investigation of PET and MPET crystallization behavior. This is due to the unstable crystal nuclei in the initial period of crystallization and the cessation of growth caused by impingement of two growing centers in the later period of crystallization. In addition, the crystallization rate can also be characterized by the half-time of crystallization  $t_{1/2}$ , which is expressed as the time cost from the onset of the crystallization to 50% completion in the crystallization process. The  $t_{1/2}$  can be obtained from Eq. (3):

$$t_{1/2} = (\ln 2 / K_t)^{1/n} \quad (3)$$

Thus,  $t_{1/2}$  is related to  $K_t$  and  $n$ . The total crystallization rate  $G$  has two components including primary nucleation rate and crystallite grown rate. The  $G$  can be obtained from Eq. (4):

$$G = (t_{1/2})^{-1} = (\ln 2 / K_t)^{-1/n} \quad (4)$$

Primary nuclei are composed of homogeneous nucleation sites formed by the polymer melt and heterogeneous nucleation sites formed from a nucleation center such as nanoparticles and impurity particles [37–39]. During the homogeneous nucleation process or the process of a spontaneous aggregation to form a three-dimensional nucleus, the nuclei growth rate is the dominating factor of the  $G$  when PET or MPET samples are crystallized at the same temperature. The crystallization rate of MPET is higher compared to neat PET due to more heterogeneous nuclei centers in MPET samples. In order to explore the crystallization temperature impact on the crystallization behavior, plots of  $\ln\{-\ln[1 - X(t)]\}$  versus  $\ln t$  at different isothermal crystallization temperatures from the primary crystallization part are shown in Fig. 8, and the related parameters are summarized

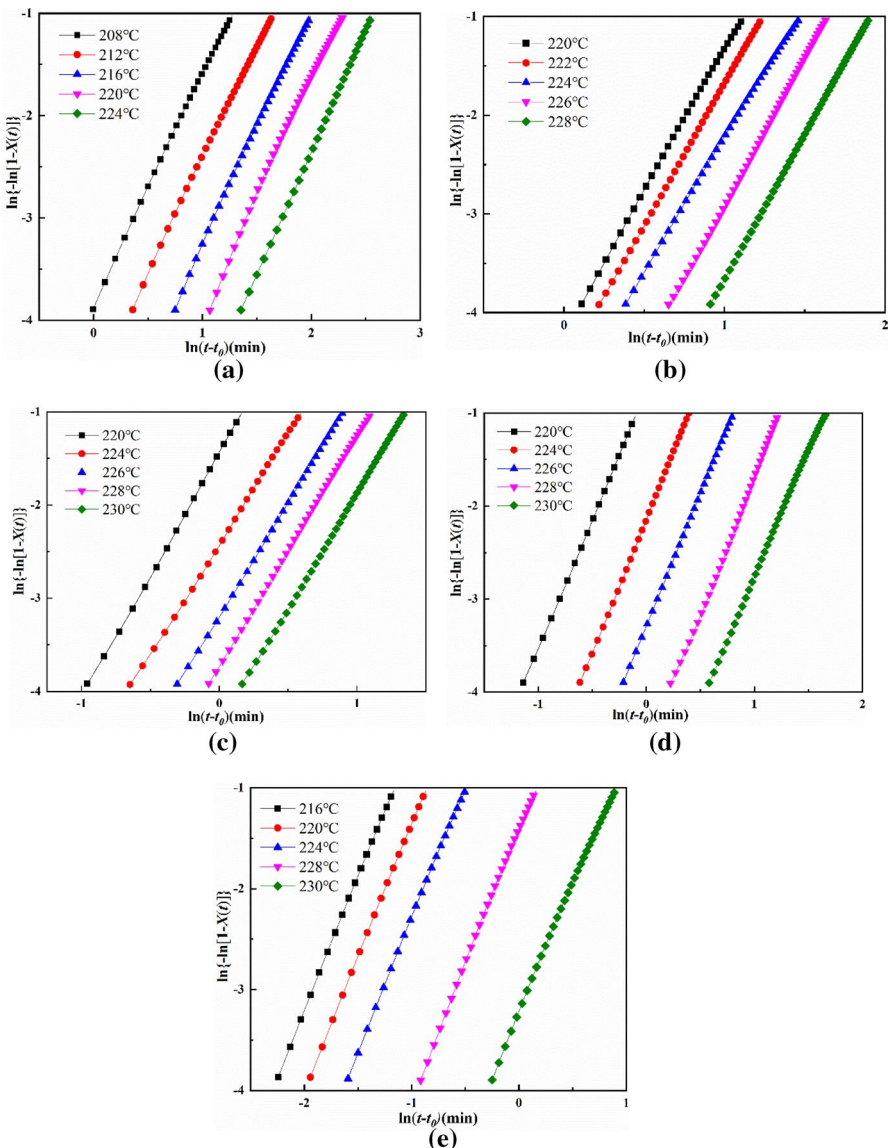


**Fig. 8** Plots of  $\ln\{-\ln[1-X(t)]\}$  versus  $\ln t$  for isothermal crystallization showing only the linear portion: PET (a); MPET-0.5 (b); MPET-1.0 (c); MPET-2.0 (d); MPET-5.0 (e)

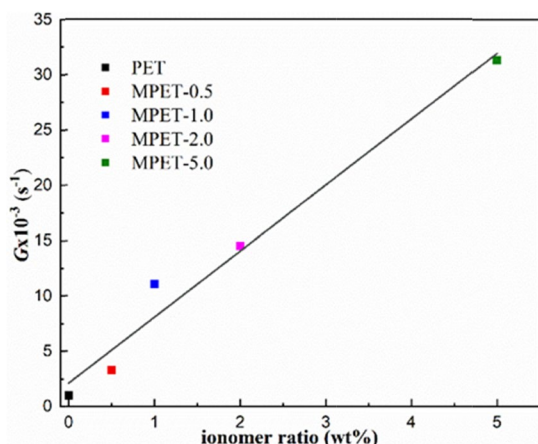
in Table 4. From Table 4, the value of  $n$  is 2.39 for neat PET at 220 °C, which is related to a confined homogeneous growth mechanism. The  $n$  of all MPET samples are bigger than neat PET at the same isothermal crystallization temperature, indicating that the crystallization of MPET samples is typical 3D crystal growth, which comply with the heterogeneous nucleation mechanism. On the one hand, it is clear that the intercept value  $\ln K_t$  decreases when the isothermal crystallization

**Table 4** Parameters of isothermal crystallization from Avrami equation

Samples	$T_c$ (°C)	$n$	$\ln K_t$	$t_{1/2}$ (s)	$G \times 10^{-3}$ ( $s^{-1}$ )
PET	208	2.23	-3.82	282	3.5
	216	2.27	-5.51	578	1.7
	220	2.38	-7.16	1029	1.0
MPET-0.5	220	2.39	-4.21	302	3.3
	224	2.48	-4.91	375	2.7
	228	2.63	-6.60	642	1.6
MPET-1.0	220	2.68	-1.45	90	11.1
	224	2.79	-2.42	125	8.0
	228	2.94	-3.73	188	5.3
MPET-2.0	220	2.78	-0.76	69	14.5
	224	2.89	-2.14	111	9.0
	228	2.96	-3.54	175	5.7
MPET-5.0	220	2.62	1.29	32	31.3
	224	2.64	0.32	46	21.7
	228	2.67	-1.40	88	11.4

temperature rises both for PET and MPET samples and the  $\ln K_t$  of MPET is larger than that of PET at the same temperature particularly. Besides, as the addition of nucleating agent increases,  $\ln K_t$  becomes larger at the same temperature. On the other hand, the  $t_{1/2}$  of MPET samples are shorter than that of PET at the same isothermal crystallization temperature. In particular, when the ionomer addition amount is only 1.0wt%, the crystallization time has been shortened from 1029 to 302 s at 220 °C, and this is associated with the difference in the crystallization mechanism for PET and MPET samples as discussed later. In addition, the crystallization rates of different samples calculated from Avrami equation at 220 °C in the isothermal crystallization are illustrated in Fig. 9. The crystallization rate

**Fig. 9** Crystallization rate versus ionomer ratio at 220 °C in the isothermal crystallization



increases with the addition of ionomers under the chosen ratios as the solid line guided by eyes in this figure. The crystallization process of MPET samples is mainly carried out via heterogeneous nucleation due to the addition of PMA-AA ionomer while neat PET mainly via homogeneous nucleation mechanism; thus, the number of heterogeneous nuclei in MPET samples is much larger compared to neat PET.

Moreover, another significant trend can be seen from Fig. 8 and parameters in Table 4. The crystallization rate constant  $K_t$  increases gradually from MPET-0.5 to MPET-5.0 with the increasing content of PMA-AA ionomer at the same isothermal crystallization temperature and the crystallization half-time  $t_{1/2}$  shifted to shorter time at this trend. These results indicate that the effect of nucleation is strengthened with more addition of PMA-AA ionomer because more PMA-AA ionomer can provide more nucleation sites for neat PET, if the nucleating agent is well dispersed. It is observed that the crystallization time becomes longer at higher isothermal crystallization temperature both for neat PET and for MPET samples. For neat PET, the  $t_{1/2}$  increased by 37 s and 113 s when the isothermal crystallization temperature  $T_c$  increased by one degree in  $T_c = 208^\circ\text{C} - 216^\circ\text{C}$  and  $T_c = 216^\circ\text{C} - 220^\circ\text{C}$ , respectively. While for MPET-1.0, the  $t_{1/2}$  increased by 18 s and 57 s each degree increase in  $T_c = 220^\circ\text{C} - 224^\circ\text{C}$  and  $T_c = 224^\circ\text{C} - 228^\circ\text{C}$ , respectively. Therefore, it is obvious that the crystallization of neat PET is more sensitive to the isothermal crystallization temperature compared to MPET samples since neat PET requires larger supercooling degree to proceed chain orientation than MPET, also as discussed above in the case of non-isothermal crystallization. It is tough for neat PET to go through three-dimensional growth at higher isothermal crystallization temperature, whereas the chain orientation movement can be accelerated by the addition of nucleation agent at higher isothermal crystallization temperature, which tends to grow in three dimension for MPET samples as the case in non-isothermal crystallization.

The crystallization thermodynamics and kinetics of PET, its blends MPET-1.0 and MPET-5.0 were further investigated by means of Hoffman–Lauritzen theory [40], which is expressed as Eq. (5):

$$G = G_0 \exp\left(-\frac{U^*}{R(T_c - T_\infty)}\right) \exp\left(-\frac{K_g}{T_c \Delta T f}\right) \quad (5)$$

In general, the total crystallization rate  $G$  is equal to the reciprocal of crystallization half-time  $1/t_{1/2}$  as shown in Eq. (4), which depends on the isothermal crystallization temperature  $T_c$ . In this equation,  $G_0$  is a factor associated with the type of polymer and  $U^*$  is the activation energy that polymer chain requires to migrate from supercooled melt to crystal phase and is equal to 6284 J/mol for neat PET [40];  $K_g$  is the nucleation rate constant and  $T_\infty$  is the temperature at which polymer chains become motionless ( $T_\infty = T_g - 30$  [41]), in which  $T_g$  is the glass transition temperature of a polymer;  $R$  is the universal gas constant,  $\Delta T$  is the supercooling temperature:  $\Delta T = T_m^0 - T_c$ , in which  $T_m^0$  is the equilibrium melting temperature expressed as the melting temperature when crystal is an infinite

pile of extended chain and  $f$  is the correction factor defined as  $f = 2T_c/(T_m^0 + T_c)$  [42]. Hoffman–Lauritzen equation usually can be transformed into a double-logarithmic equation form as shown in Eq. (6):

$$\ln G + \frac{U^*}{R(T_c - T_\infty)} = \ln G_0 - \frac{K_g}{T_c \Delta Tf} \quad (6)$$

The equilibrium melting temperature  $T_m^0$  thus can be determined according to the linear relation between the melting temperature  $T_m$  and isothermal crystallization temperature  $T_c$  based on Hoffman and Weeks plots [43].  $T_m$  can be measured by reheating the samples at a rate of 10 °C/min after complete isothermal crystallization and the intersection point in the linear extrapolation of  $T_m$  versus  $T_c$  where  $T_m = T_c$  is  $T_m^0$ . The value of  $T_m^0$  for neat PET is 548.19 K based on plots of  $T_m$  versus  $T_c$  as shown in Fig. 10, which approaches to the value of 547.15 K as reported in the literature [44]. The calculated values of  $T_m^0$  for MPET samples with the addition of PMA-AA-Na are approximately 540 K, which is slightly lower than that of neat PET. This may be attributed to the different isothermal crystallization temperature ranges selected to investigate the isothermal crystallization kinetics of PET and MPET samples [45, 46].

The isothermal crystallization of PET, MPET-1.0, and MPET-5.0 at various temperatures was investigated for further study, and the corresponding  $t_{1/2}$  values are calculated from Eq. (3) and summarized in Table 4. It is observed that the PMA-AA ionomer promotes PET crystallization at a greater extent under identical conditions. Figure 11 illustrates the linear lines related to the plot of  $\ln G + U^*/R(T_c - T_\infty)$  vs  $1/(T_c \Delta Tf)$ . The value of  $K_g$  can be obtained from the slope of the straight lines and summarized in Table 5. For a heterogeneous nucleation, the nucleation constant  $K_g$  can be expressed as Eq. (7):

**Fig. 10** Hoffman–Weeks plots of the melting temperature  $T_m$  versus isothermal crystallization temperature  $T_c$  for PET, MPET-1.0, MPET-5.0 to determine the equilibrium melting temperature  $T_m^0$

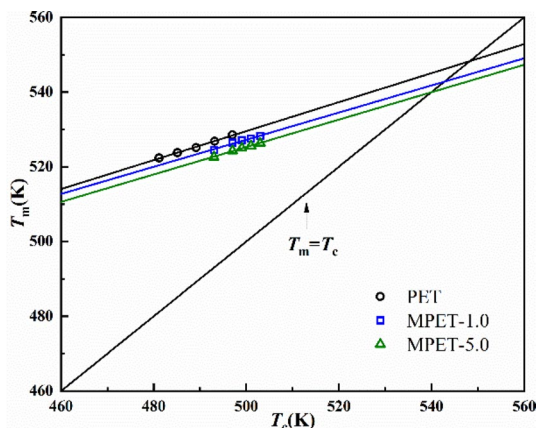


**Fig. 11** Lauritzen–Hoffman plots of  $\ln G + U^*/R(T_c - T_\infty)$  versus  $1/T_c \Delta Tf$  for isothermal crystallization of PET, MPET-1.0 and MPET-5.0

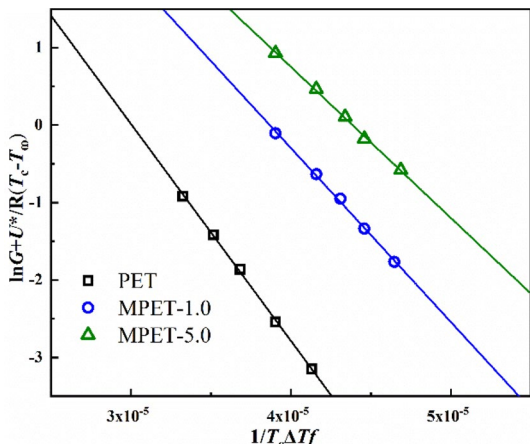


**Table 5** Kinetic parameter  $K_g$  and fold surface free energy  $\sigma_e$  of PET, MPET-1.0, and MPET-5.0

	PET	MPET-1.0	MPET-5.0
$K_g (10^5)$	2.80	2.22	1.99
$\sigma_e (\text{J/m}^{-2})$	110.0	44.6	38.8

$$K_g = \frac{zb\sigma\sigma_e T_m^0}{k_B \Delta H_m^0} \quad (7)$$

$z$  is related to the crystallization regimes [41] with the value of 4 for crystallization regime I and III while 2 for regime II;  $b$  characterizes the distance between two adjacent fold planes and the suitable growth face for PET is the (0 1 0) plane where  $b = 5.95\text{\AA}$ ;  $\sigma$  and  $\sigma_e$  are lateral surface free energy and fold surface free energy, respectively, and  $k_B$  is the Boltzmann constant ( $k_B = 1.38 \times 10^{-23} \text{ J/K}$ ).  $\sigma$  and  $\sigma_e$  can be calculated by the empirical Eqs. (8) and (9) [35, 47]:

$$\sigma = \alpha \times \Delta H_m^0 \times (a_0 b_0)^{1/2} \quad (8)$$

$$\sigma_e = \frac{K_g}{T_m^0} \frac{k_B}{4b\alpha(a_0 b_0)^{1/2}} \quad (9)$$

where  $\Delta H_m^0$  means the equilibrium melting enthalpy ( $\Delta H_m^0 = 2.1 \times 10^8 \text{ J/m}^3$ ),  $\alpha = 0.11$  [42],  $a_0$  and  $b_0$  are the unit cell dimensions are  $4.57\text{\AA}$  and  $5.95\text{\AA}$  for PET, respectively [48]. PET crystallization kinetics obeys regime I ( $z = 4$ ) when the temperature is above 490 K and MPET samples in this work belong to this regime as reported in the literature [41]. While PET crystallization follows the regime II ( $z = 2$ ) when the temperature is below 490 K and neat PET is part of this regime. The fold surface free energy  $\sigma_e$  is a significant factor to evaluate the nucleating effect of an addition agent and an effective nucleating agent can reduce  $\sigma_e$  of polymer

[49, 50]. The  $\sigma_e$  of neat PET was calculated to be  $110.0 \text{ J/m}^{-2}$  through Eq. (9), while MPET-1.0 and MPET-5.0 reduce to  $44.6 \text{ J/m}^{-2}$  and  $38.8 \text{ J/m}^{-2}$ , respectively, as summarized in Table 5. In general, the smaller fold surface energy of a polymer represents the higher crystallization rate. The addition of PMA-AA ionomer can reduce the fold surface free energy  $\sigma_e$  by providing more nucleation sites and improving the crystallization rate of PET as a result. Moreover,  $\sigma_e$  decreases gradually with increasing the content of PMA-AA ionomer, indicating the superior compatibility between PMA-AA ionomer and PET.

### Dispersion and crystallization morphology of PET/ionomer blends

The dispersion of the nucleating agent is the key to improve the nucleation efficiency of polymer crystallization. To investigate the dispersion of ionomer in PET matrix, MPET-1.0 was chosen as the typical blend for further study. The fractured surfaces of MPET-1.0 are shown in Fig. 12, while MPET blends with other ionomer ratios are shown in Fig. S1 and all annealing samples are of 0.1–0.2 mm thickness. The fractured surfaces of samples were covered with gold via a spraying machine attached to Ultra-55 type SEM and the physical vapor depositing time of spraying was 90–120 s. SEM morphology observed at the

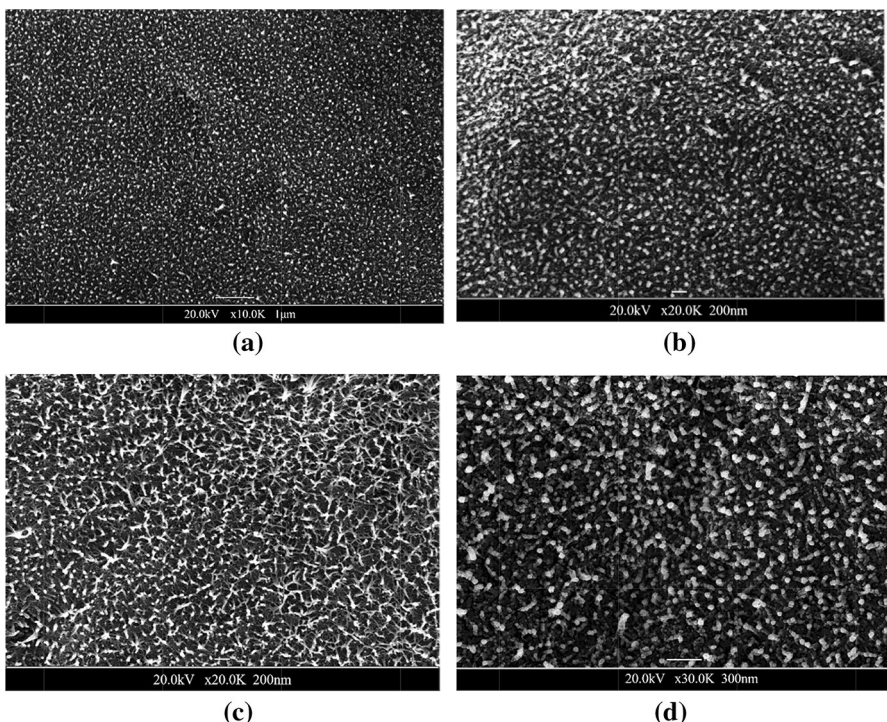


**Fig. 12** SEM morphology of PMA-AA ionomer dispersing in fractured MPET-1.0 film surface with 0.1–0.2 mm thickness at different magnifications (a–d), (b) and (c) are different areas of the sample

voltage of 20 kV clearly showed that ordered texture morphology was formed on the fractured surface of MPET-1.0, which reflected that the PMA-AA ionomer is homogeneously dispersed in PET and allow the molecular chain of PET to crystallize in order. Obviously, the chemical reaction between ionomer and molecular chain of PET enhanced the affinity between PET and ionomer, which had a significant effect on promoting PMA-AA ionomer to disperse well. PET produced vivid ordered patterns due to the homogeneous disperse of ionomer in the matrix. The pictures in Fig. 12 are the samples at different magnifications, and it is confirmed that the ionomer is very uniformly dispersed in the PET matrix and lead to the crystallization of PET via heterogeneous nucleation as shown in Fig. S1.

The superior dispersion of the ionomer accelerated the nucleation and growth of crystals in the isothermal crystallization process of PET. Firstly, a film sample was sandwiched between two transparent microscope coverslips and then placed on the hot stage with nitrogen. Secondly, the film sample was heated to 285 °C at the rate of 10 °C/min and pressed to a thin film about 10 μm in thickness and maintained at 285 °C for 5 min to erase the previous thermal history as the measurements in DSC. Finally, the thin film was quenched rapidly to the target isothermal crystallization temperature  $T_c$  at a cooling rate of 100 °C/min and hold at that temperature to complete the crystallization of samples where the growth of spherulites with time was recorded by a CCD camera.

Figure 13 presents the crystalline morphologies of neat PET and MPET samples under isothermal crystallization at 220 °C to investigate the spherulite growth process with time. Figure 13a–d are neat PET and Fig. 13e–h are MPET-1.0, while images of MPET with other ionomer ratios are shown in Fig. S2. The sizes of spherulites were rather big and irregular for neat PET, while the sizes of spherulites were small and uniform for the MPET samples due to the addition of 1.0 wt% of PMA-AA-Na. As discussed above, PMA-AA ionomer acts as a heterogeneous nucleating agent to increase the crystallization rate of neat PET and reduce the distance between spherulites, leading to the formation of more perfect crystals in MPET samples compared to neat PET. When the isothermal crystallization time is 90 s, only few spherulites can be observed in PET, whereas large amounts of spherulites can be seen in MPET-1.0. In general, nucleation sites occur spontaneously and randomly in homogeneous nucleation, which results in the random distribution of nucleation sites and relatively slow growth at those sites. Figure 13 shows that the spherulite sizes of PET rapidly decrease with the addition of 1.0% PMA-AA-Na, which indicates that PMA-AA ionomer provided considerable nucleation sites and increased the density of nucleus, thus accelerating the crystallization rate of PET. It is obvious that the growth of the spherulite crystals of PET is rather slower than that of MPET-1.0. The spherulite crystals in PET/PMA-AA-Na samples grow instantaneously and subsequently are limited to grow by impingement of adjacent spherulites due to the addition of a large quantity of nucleation sites via PMA-AA ionomer. For PET, the crystal stopped growing until 360 s in isothermal crystallization process at 220 °C while for MPET-1.0, the crystal stopped growing about at 210 s at 220 °C reflecting that PMA-AA ionomer indeed accelerates the crystallization rate of PET and exhibits a dose-dependent manner in Fig. S2 as discussed in the DSC measurement above.

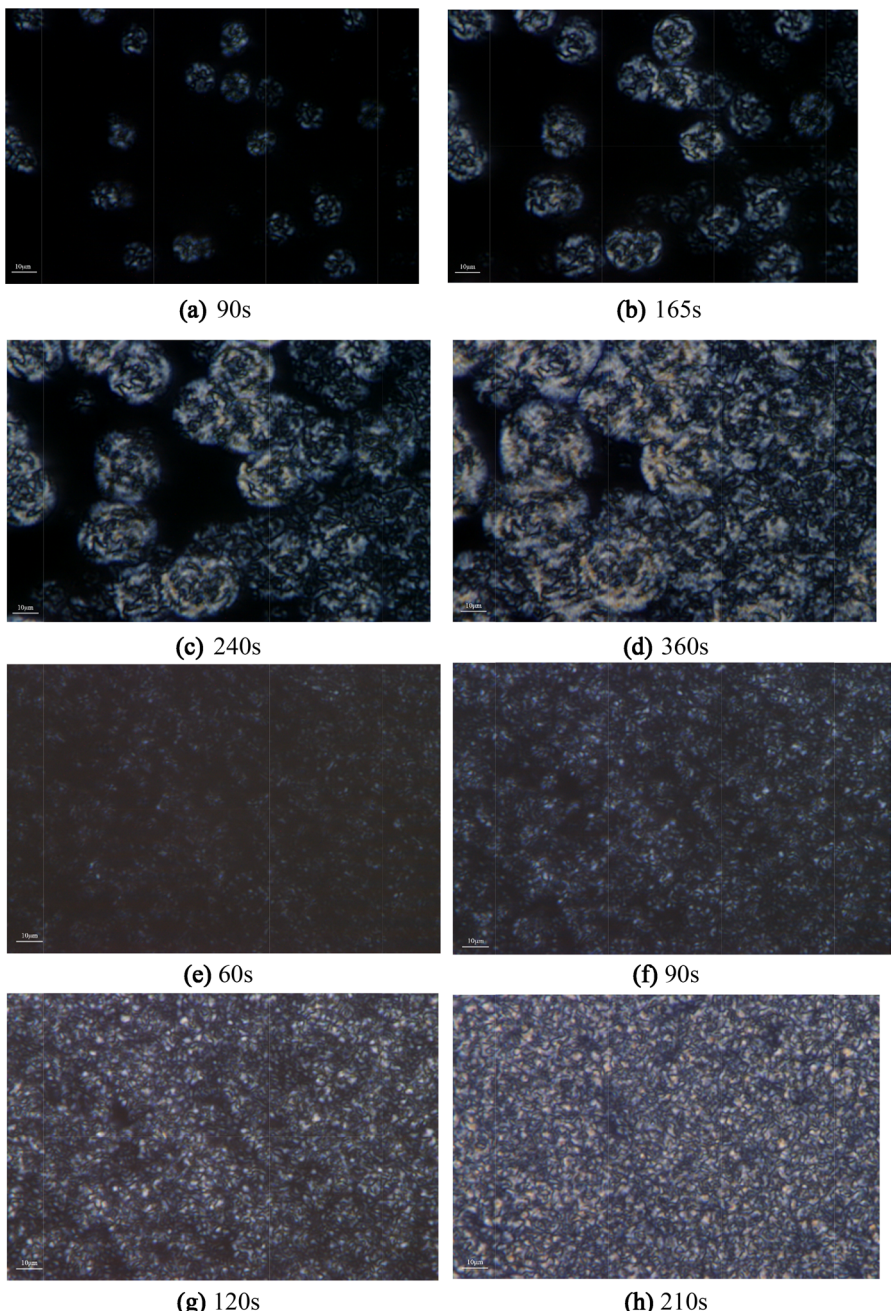


**Fig. 13** The time evolution of crystal morphologies with POM pictures of PET (a–d), MPET-1.0 (e–h) isothermally crystallized at 220 °C for 5 min

## Thermal stability behavior of PET and MPET blends

Figure 14 shows the TGA and its differential curves of the neat PET and the MPET blends. All degradation temperatures are determined by the initial extrapolation method on the figure. The samples of about 3 mg was heated from room temperature to 800 °C at the heating rate of 10 °C/min under a nitrogen atmosphere. As shown in Fig. 14, during the TGA analysis, it is clearly shown a two-stage decomposition and the degradation temperature of PET/ionomer blends was above 350 °C. Therefore, it is demonstrated that the ionomer maintains a solid state without degradation, thereby providing nucleating sites for neat PET. The first stage of decomposition for neat PET is due to overlap of two decomposition processes according to the reported literature [51]. The first degradation process is mainly attributed to the molecular chain degradation through chain-end initiated mechanism, and the second degradation process is due to the degradation of the products formed during the first process. For neat PET, the second degradation stage in the temperature between 520–650 °C is because of the decomposition of thermally stable products formed during the first degradation stage. For MPET blend samples, the first stage of decomposition was similar to neat PET where the decomposition is attributed to both PET matrix and ionomer, while the second decomposition stage for MPET samples was broader than that of neat PET and the broadness extended as the increase in ionomer content. The second decomposition stage proceeded in the temperature range of 540–750 °C for MPET-5.0 that could be due to the formation of the considerable amounts of the clusters between ionomer and the functional groups of PET chain, which goes through a slow decomposition in a wide temperature range. The calculated data of TGA analysis such as temperature at 1.0 wt% weight loss and at 5.0 wt% weight loss, decomposition onset, the weight loss during second decomposition and the residue mass at 700 °C are summarized in Table 6. It is obvious that the temperatures at 1.0 wt% and 5.0 wt% weight loss and the decomposition onset for the MPET are lower than that of neat PET. This could be due to the degradation of the short PET chain caused by the chain scission after the reaction between PET and ionomer. In

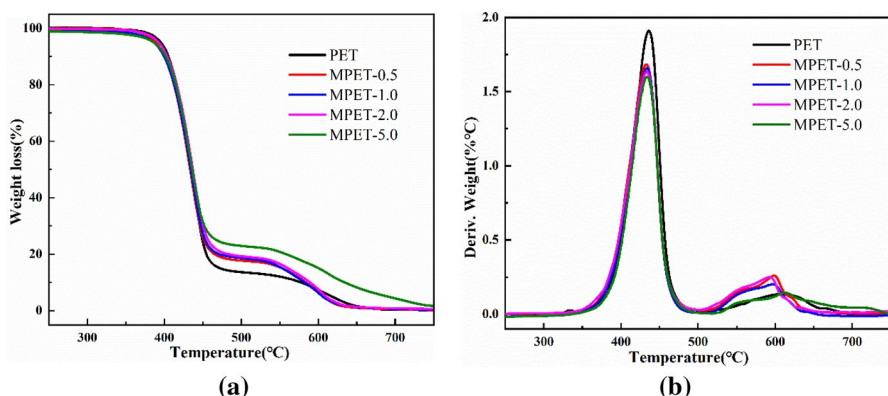


**Fig. 14** TGA (a) and their differential curves (b) of PET and MPET blends

**Table 6** The results of TGA on PET and MPET blends

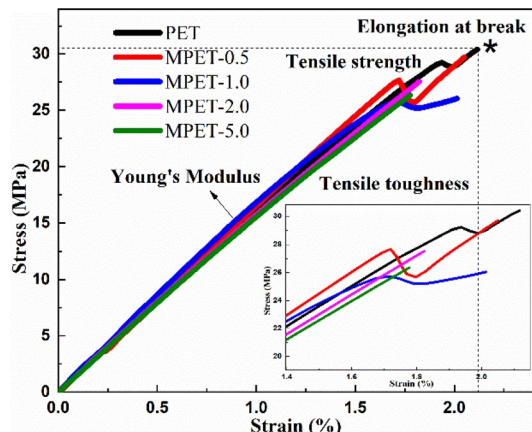
Sample	Temp. <sup>a</sup> (°C)	Temp. <sup>b</sup> (°C)	Decomposition onset	Weight loss <sup>c</sup> (%)	Residual mass <sup>d</sup> (%)
PET	372	395	413	12.3	0.1
MPET-0.5	369	392	410	16.6	0.2
MPET-1.0	363	387	408	17.1	0.3
MPET-2.0	352	384	407	18.2	0.7
MPET-5.0	345	385	410	21.8	1.6

<sup>a</sup>Temperature at 1.0 wt% weight loss, <sup>b</sup>temperature at 5.0 wt% weight loss, <sup>c</sup>weight loss during second decomposition, <sup>d</sup>residual mass at 700 °C

addition, when adding only 1.0 wt% ionomer, no significant drop at 1.0 wt% and 5.0 wt% weight loss was observed.

### Mechanical properties of PET and MPET blends

The mechanical properties for PET and MPET blends were also investigated. The stress–strain curves of all samples are shown in Fig. 15. In the stress–strain curve, the value of Young's modulus, which is the slope of the curve, indicates the stiffness of a sample, while the value of elongation at break represents the brittleness of the sample and the value of stress at break is tensile strength. Moreover, the area under the strain–stress curve reveals the tensile toughness of the sample, which is influenced both by Young's modulus and elongation at break. Young's modulus, namely tensile modulus, and the elongation at break of PET and MPET samples with the incorporation of ionomer, is shown in Fig. 16, and the average parameters are recorded in Table 7. When the addition of PMA-AA ionomer is less than 1.0 wt%, the tensile modulus and tensile strength of MPET samples are enhanced with the increasing content of the ionomer, which can be attributed to the increase in

**Fig. 15** Stress–strain curves for PET and MPET blends

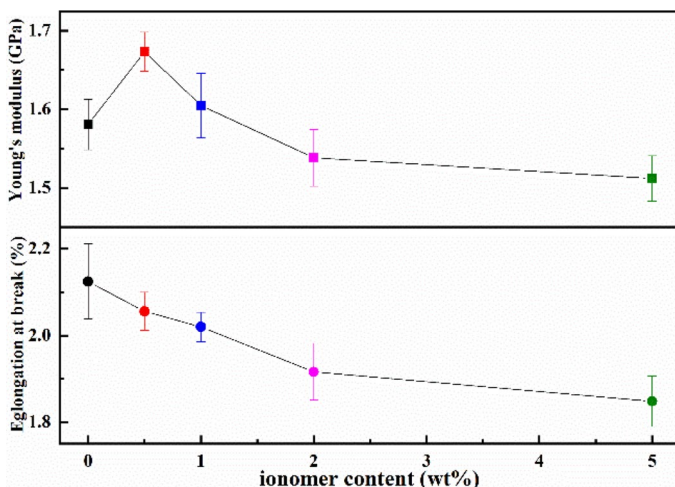


**Fig. 16** Mechanical properties of pure PET and MPET blends

**Table 7** Values of intrinsic viscosity and mechanical parameters for PET and MPET blends

	PET	MPET-0.5	MPET-1.0	MPET-2.0	MPET-5.0
Intrinsic viscosity (dL/g)	0.64	0.65	0.63	0.59	0.55
Young's modulus (GPa)	1.58	1.67	1.61	1.53	1.51
Elongation at break (%)	2.13	2.06	2.02	1.92	1.85
Tensile strength (MPa)	28.5	30.4	28.6	27.9	26.1
Tensile toughness (MPa)	31.1	31.3	29.1	24.5	22.1

crystallinity degree of PET. The influence on crystallinity directly improves the tensile strength and tensile toughness of the blends, and these samples exhibit ductile fracture behavior. However, for the blends with higher ionomer content as MPET-2.0 and MPET-5.0, the addition of excessive ionomer will cause slight scission of the PET chain and the decrease of the molecular weight of PET as seen in the value of intrinsic viscosity. Therefore, the tensile toughness of MPET-2.0 and MPET-5.0 shift to lower value and the samples exhibit like brittle materials while maintaining a certain tensile strength. The excellent mechanical properties of MPET-0.5 and MPET-1.0 blends are associated with the superior nucleating effect of PMA-AA ionomer, which induces an improvement in crystallinity and homogeneity of the blends.

### Oxygen barrier properties of PET and MPET blends

The polymer crystallinity affects the transfer of gases directly, which is one of the main factors influencing the storage of products through packaging material. The

**Fig. 17** Oxygen transmission rate for PET and MPET blends

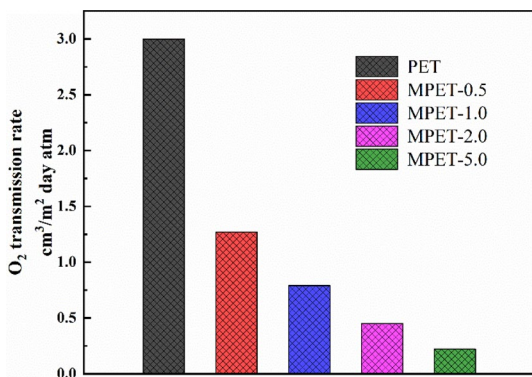


**Table 8** Values of crystallinity and oxygen transmission rate for PET and MPET blends

	PET	MPET-0.5	MPET-1.0	MPET-2.0	MPET-5.0
X <sub>c</sub> %	29.5	36.0	37.8	39.0	40.1
O <sub>2</sub> transmission rate (cm <sup>3</sup> /m <sup>2</sup> day atm)	3.00	1.27	0.79	0.45	0.22

oxygen permeability of MPET film samples exhibited better oxygen barrier properties than neat PET in a dry state with a relative humidity of 0. First of all, the permeated cell was flushed with nitrogen gas with a purity of 99.99% to condition samples over many hours. Secondly, oxygen gas with purity of 99.99% was introduced into the upstream chamber. The oxygen flux through the 38.48 cm<sup>2</sup> film in the exposed area was recorded until a steady state was reached. All measurements were taken at the temperature of 23 °C under atmospheric pressure and at least three times to acquire the average value.

As shown in Fig. 17 and Table 8, the oxygen transmission rate (OTR) value of neat PET is 3.00 cm<sup>3</sup> m<sup>-2</sup> day<sup>-1</sup> atm<sup>-1</sup>, while the OTR values of MPET-0.5, MPET-1.0, MPET-2.0 and MPET-5.0 were reduced apparently to 1.27, 0.79, 0.45, and 0.22 cm<sup>3</sup> m<sup>-2</sup> day<sup>-1</sup> atm<sup>-1</sup>, respectively. The improvement of gas barrier properties is meaningful for MPET blends to be applied in product packaging. The oxygen transmission rate of PET is decreased by more than 70% after adding only 1.0 wt% ionomer, which can be attributed to the increase in crystallization degree and finer spherulite size, resulting in hindered gas transfer and increased diffusion pathways. In addition, MPET blends with more content of PMA-AA ionomer have shorter chains, resulting in more chain end than that of neat PET. These chain ends allow more reduction in the free volume due to the high affinity for water molecules, which leads to a decrease in the oxygen permeation. It is proved that PMA-AA ionomer is an efficient nucleation agent, and MPET blends show extremely low oxygen permeability, which has great significance for food packaging. By improving the O<sub>2</sub> barrier properties of PET, it is possible to package sensitive products that might lose their organoleptic and nutritional qualities or color due to oxidation.

## Conclusion

In this study, we focused on the improvement of crystallization behavior and properties of neat PET. In summary, the heterogeneous nucleation is more likely to proceed at lower supercooling degree compared to homogeneous nucleation. We discover that PMA-AA ionomer can be used as a new type of nucleating agent to improve the crystallization behavior of PET. The addition of PMA-AA ionomers can change the nucleation type and decrease the spherulite size, leading to a considerable reduction of the crystallization time and an obvious increase on the crystallization temperature of neat PET. Moreover, with more content of PMA-AA-Na, the half-crystallization time of MPET blends becomes shorter, indicating that PMA-AA-Na has a superior nucleating effect. The incorporation of PMA-AA-Na reduces the nucleation and surface free energy of the polymer chains, thus reducing the energy barrier in the process of nucleation. PMA-AA ionomers are dispersed in the PET matrix homogeneously and thus accelerating the nucleation process of MPET blends. Furthermore, the incorporation of PMA-AA-Na improves the thermal stability, mechanical properties, and gas barrier of MPET blends significantly. At the same time, we found that this work is worthy of further study and the PET/ionomer blends have great industrialization potential. Therefore, the crystallized MPET blends have possible applications in food packaging and engineering industries.

**Supplementary Information** The online version contains supplementary material available at <https://doi.org/10.1007/s00289-021-03672-3>.

**Acknowledgments** The authors thank the financial support from the National Natural Science Foundation of China (Grant Nos. 21774027, 21973017, and 21534002).

## References

1. Fan C, Wan C, Gao F et al (2015) Extrusion foaming of poly(ethylene terephthalate) with carbon dioxide based on rheology analysis. *J Cell Plast* 52:277. <https://doi.org/10.1177/0021955x14566085>
2. Ou CF, Li WC, Chen YH (2002) Thermal and crystallization characteristics of poly(ethylene terephthalate) with poly(oxybenzoate-p-trimethylene terephthalate) copolymer. *J Appl Polym Sci* 86:1599. <https://doi.org/10.1002/app.11046>
3. Imai Y, Nishimura S, Abe E et al (2002) High-modules poly(ethylene terephthalate)/expandable fluorine mica nanocomposites with a novel reactive compatibilizer. *Chem Mater* 14:477. <https://doi.org/10.1021/cm010408a>
4. Ge Q, Ding XJ, Wu G, Liang S, Wu SZ (2007) Study on the microstructure and mechanical properties of PET and PET/PTT blends. *Key Eng Mater* 340–341:1085
5. Kint DPR, Muñoz-Guerra S (2003) Modification of the thermal properties and crystallization behaviour of poly(ethylene terephthalate) by copolymerization. *Polym Int* 52:321. <https://doi.org/10.1002/pi.1175>
6. Misra E, Basavarajaiah S, Kumar KR, Ravi P (2000) Effect of recycling on the properties of poly(ethylene terephthalate) films. *Polym Int* 49:1636. [https://doi.org/10.1002/1097-0126\(200012\)49:12%3c1636::Aid-pi574%3e3.0.Co;2-3](https://doi.org/10.1002/1097-0126(200012)49:12%3c1636::Aid-pi574%3e3.0.Co;2-3)
7. Kravets L, Dmitriev S, Gilman A, Drachev A, Dinescu G (2005) Water permeability of poly(ethylene terephthalate) track membranes modified by DC discharge plasma polymerization of dimethylaniline. *J Membr Sci* 263:127. <https://doi.org/10.1016/j.memsci.2005.04.012>

8. Buckley CP, Jones DC, Jones DP (1996) Hot-drawing of poly(ethylene terephthalate) under biaxial stress: application of a three-dimensional glass-rubber constitutive model. *Polymer* 37:2403. [https://doi.org/10.1016/0032-3861\(96\)85352-3](https://doi.org/10.1016/0032-3861(96)85352-3)
9. Alfonso GC, Verdona MP, Wasiak A (1978) Crystallization kinetics of oriented poly(ethylene terephthalate) from the glassy state. *Polymer* 19:711. [https://doi.org/10.1016/0032-3861\(78\)90128-3](https://doi.org/10.1016/0032-3861(78)90128-3)
10. Kuczynski B, Geyer R (2010) Material flow analysis of polyethylene terephthalate in the US, 1996–2007. *Resour Conserv Recycl* 54:1161. <https://doi.org/10.1016/j.resconrec.2010.03.013>
11. Yeh GSY, Geil PH (1967) Crystallization of polyethylene terephthalate from the glassy amorphous state. *J Macromol Sci B* 1:235. <https://doi.org/10.1080/00222346708212777>
12. Ke YC, Wu TB, Xia YF (2007) The nucleation, crystallization and dispersion behavior of PET-monodisperse  $\text{SiO}_2$  composites. *Polymer* 48:3324. <https://doi.org/10.1016/j.polymer.2007.03.059>
13. Ou CF, Ho MT, Lin JR (2003) The nucleating effect of montmorillonite on crystallization of PET/montmorillonite nanocomposite. *J Polym Res* 10:127. <https://doi.org/10.1023/a:1024981914234>
14. Legras R, Bailly C, Daumerie M et al (1984) Chemical nucleation, a new concept applied to the mechanism of action of organic acid salts on the crystallization of polyethylene terephthalate and bisphenol-A polycarbonate. *Polymer* 25:835. [https://doi.org/10.1016/0032-3861\(84\)90015-6](https://doi.org/10.1016/0032-3861(84)90015-6)
15. Garcia D (1984) Heterogeneous nucleation of poly(ethylene-terephthalate). *J Polym Sci Pol Phys* 22:2063. <https://doi.org/10.1002/pol.1984.180221206>
16. He Z, Zhang Z, Asare-Yeboah K, Bi S, Chen J, Li D (2021) Crystal growth of small-molecule organic semiconductors with nucleation additive. *Curr Appl Phys* 21:107. <https://doi.org/10.1016/j.cap.2020.10.014>
17. He Z, Chen J, Keum JK, Szulczewski G, Li D (2014) Improving performance of TIPS pentacene-based organic thin film transistors with small-molecule additives. *Org Electron* 15:150. <https://doi.org/10.1016/j.orgel.2013.11.004>
18. Ma Y, Yang G, Xie L (2014) Morphology, nonisothermal crystallization behavior and mechanical properties of polypropylene modified by ionomers. *J Macromol Sci B* 53:1829. <https://doi.org/10.1080/00222348.2014.970845>
19. Tang S, Xin Z (2009) Structural effects of ionomers on the morphology, isothermal crystallization kinetics and melting behaviors of PET/ionomers. *Polymer* 50:1054. <https://doi.org/10.1016/j.polym.2008.12.015>
20. Zhang L, Brostowitz NR, Cavicchi KA, Weiss RA (2014) Perspective: ionomer research and applications. *Macromol React Eng* 8:81. <https://doi.org/10.1002/mren.201300181>
21. Ju L, Pretelt J, Chen T et al (2018) Synthesis and characterization of phosphonated poly(ethylene terephthalate) ionomers. *Polymer* 151:154. <https://doi.org/10.1016/j.polymer.2018.07.065>
22. Yu Y, Yu YL, Jin M, Bu HS (2000) Nucleation mechanism and crystallization behavior of poly(ethylene terephthalate) containing ionomers. *Macromol Chem Phys* 201:1894. [https://doi.org/10.1002/1521-3935\(20000901\)201:14%3c1894::Aid-macp1894%3e3.0.Co;2-q](https://doi.org/10.1002/1521-3935(20000901)201:14%3c1894::Aid-macp1894%3e3.0.Co;2-q)
23. Yu Y, Bu HS (2001) Crystallization behavior of poly(ethylene terephthalate) modified by ionomers. *Macromol Chem Phys* 202:421. [https://doi.org/10.1002/1521-3935\(20010201\)202:3%3c421::Aid-macp421%3e3.0.Co;2-v](https://doi.org/10.1002/1521-3935(20010201)202:3%3c421::Aid-macp421%3e3.0.Co;2-v)
24. Kalfoglou NK, Skafidas DS (1994) Crystallization processes in poly(ethylene terephthalate) as modified by polymer additives and fiber reinforcement. *Eur Polym J* 30:933. [https://doi.org/10.1016/0014-3057\(94\)90027-2](https://doi.org/10.1016/0014-3057(94)90027-2)
25. Xing SL, Tang P, Yang YL (2015) Poly(styrene-co-maleic anhydride) ionomers as nucleating agent on the crystallization behavior of poly(ethylene terephthalate). *J Appl Polym Sci* 132:41240. <https://doi.org/10.1002/app.41240>
26. Xing S, Li R, Tang P (2015) Synthesis and microphase separation of PS-b-P(MA-alt-St) block copolymers and their ionomers for the design of polymer crystallization nucleation agents. *Macromol Chem Phys* 216:301. <https://doi.org/10.1002/macp.201400444>
27. Ramesan MT, Lee DS (2008) The effect of block copolymer and its ionomer on the crystallization behaviour of poly(ethylene terephthalate). *Iran Polym J* 17:281
28. Rivas BL, Seguel CV (1999) Poly(acrylic acid-co-maleic acid)-metal complexes with copper(II), cobalt(II), and nickel(II)—Synthesis, characterization and structure of its metal chelates. *Polyhedron* 18:2511. [https://doi.org/10.1016/s0277-5387\(99\)00149-7](https://doi.org/10.1016/s0277-5387(99)00149-7)
29. Vauclair C, Schaezsel P, Nobrega R, Habert C (2002) Dehydration of light oil by pervaporation using poly(vinyl alcohol)-poly(acrylic acid-co-maleic acid) membranes. *J Appl Polym Sci* 86:1709. <https://doi.org/10.1002/app.11076>

30. Abyan M, Bertorelle F, Fery-Forgues S (2005) Use of linear polymers to control the preparation of luminescent organic microcrystals. *Langmuir* 21:6030. <https://doi.org/10.1021/la046877j>
31. Taniguchi A, Cakmak M (2004) The suppression of strain induced crystallization in PET through sub micron TiO<sub>2</sub> particle incorporation. *Polymer* 45:6647. <https://doi.org/10.1016/j.polymer.2004.06.056>
32. Zhang H, Zhang Y, Guo W, Xu D, Wu C (2008) Thermal properties and morphology of recycled poly(ethylene terephthalate)/maleic anhydride grafted linear low-density polyethylene blends. *J Appl Polym Sci* 109:3546. <https://doi.org/10.1002/app.28456>
33. Macknight WJ, Earnest TR (1981) The structure and properties of ionomers. *J Polym Sci Macromol Rev* 16:41
34. Friedman HL (1964) Kinetics of thermal degradation of char-forming plastics from thermogravimetry .Application to phenolic plastic. *J Polym Sci Part C-Polymer Symposium* 6:183
35. Avrami M (1939) Kinetics of phase change I—General theory. *J Chem Phys* 7:1103. <https://doi.org/10.1063/1.1750380>
36. Avrami M (1941) Granulation, phase change, and microstructure—kinetics of phase change III. *J Chem Phys* 9:177. <https://doi.org/10.1063/1.1750872>
37. Bassett DC (2006) Linear nucleation of polymers. *Polymer* 47:5221. <https://doi.org/10.1016/j.polym.2006.05.028>
38. Imai M, Kaji K (2006) Polymer crystallization from the metastable melt: the formation mechanism of spherulites. *Polymer* 47:5544. <https://doi.org/10.1016/j.polymer.2005.07.109>
39. Mamun A, Umemoto S, Ishihara N, Okui N (2006) Influence of thermal history on primary nucleation and crystal growth rates of isotactic polystyrene. *Polymer* 47:5531. <https://doi.org/10.1016/j.polymer.2005.04.110>
40. Hoffman JD, Davis GT, Lauritzen JI (1976) Treatise on Solid State Chemistry
41. Long Y, Shanks RA, Stachurski ZH (1995) Kinetics of polymer crystallisation. *Prog Mater Sci* 20:651
42. Lu XF, Hay JN (2001) Isothermal crystallization kinetics and melting behaviour of poly(ethylene terephthalate). *Polymer* 42:9423. [https://doi.org/10.1016/s0032-3861\(01\)00502-x](https://doi.org/10.1016/s0032-3861(01)00502-x)
43. Hoffman JD, Weeks JJ (1962) Melting process and the equilibrium melting temperature of polychlorotrifluoroethylene. *J Res Nat Bur Stand Sec* 66A:13. <https://doi.org/10.6028/jres.066A.003>
44. Reinsch VE, Rebenfeld L (1994) Crystallization processes in poly(ethylene terephthalate) as modified by polymer additives and fiber reinforcement. *J Appl Polym Sci* 52:649. <https://doi.org/10.1002/app.1994.070520508>
45. Jiang XL, Luo SJ, Sun K, Chen XD (2007) Effect of nucleating agents on crystallization kinetics of PET. *Express Polym Lett* 1:245. <https://doi.org/10.3144/expresspolymlett.2007.37>
46. Deshpande VD, Jape S (2010) Isothermal crystallization kinetics of anhydrous sodium acetate nucleated poly(ethylene terephthalate). *J Appl Polym Sci* 116:3541. <https://doi.org/10.1002/app.31891>
47. Bt L, Marić M, (2010) One-step poly(styrene-alt-maleic anhydride)-block-poly(styrene) copolymers with highly alternating styrene/maleic anhydride sequences are possible by nitroxide-mediated polymerization. *Macromolecules* 43:879. <https://doi.org/10.1021/ma902234t>
48. Yamashit Y (1965) Single crystals of poly(ethylene terephthalate). *J Polym Sci Part A-General Papers* 3:81. <https://doi.org/10.1002/pol.1965.100030110>
49. Yu B, Wang X, Qian X et al (2014) Functionalized graphene oxide/phosphoramido oligomer hybrids flame retardant prepared via in situ polymerization for improving the fire safety of polypropylene. *RSC Adv.* <https://doi.org/10.1039/c3ra45945d>
50. Cao L, Su D, Su Z, Chen X (2014) Fabrication of multiwalled carbon nanotube/polypropylene conductive fibrous membranes by melt electrospinning. *Ind Eng Chem Res* 53:2308. <https://doi.org/10.1021/ie403746p>
51. Wang XS, Li XG, Yan DY (2000) Thermal decomposition kinetics of poly(trimethylene terephthalate). *Polym Degrad Stabil* 69:361. [https://doi.org/10.1016/s0141-3910\(00\)00083-5](https://doi.org/10.1016/s0141-3910(00)00083-5)

**Publisher's Note** Springer Nature remains neutral with regard to jurisdictional claims in published maps and institutional affiliations.